ELSEVIER

Biophysical Chemistry 128 (2007) 215–230

Biophysical Chemistry

http://www.elsevier.com/locate/biophyschem

# Molecular dynamics simulations of pea (*Pisum sativum*) lectin structure with octyl glucoside detergents: The ligand interactions and dynamics

Praveen Konidala [a], Bernd Niemeyer [a,b,*]

[a] *Institute of Thermodynamics, Helmut-Schmidt-University / University of the Federal Armed Forces Hamburg, Holstenhofweg 85, D-22043 Hamburg, Germany*
[b] *Institute for Coastal Research, Marine Bioanalytical Chemistry, GKSS Research Center, D-21502 Geesthacht, Germany*

Received 21 January 2007; received in revised form 18 April 2007; accepted 18 April 2007
Available online 24 April 2007

**Abstract**

The mitogenic pea (*Pisum sativum*) lectin is a legume protein of non-immunoglobulin nature capable of specific recognition of glucose derivatives without altering its structure. Molecular dynamics simulations were performed in a realistic environment to investigate the structure and interaction properties of pea lectin with various concentrations of *n*-octyl-β-D-glucopyranoside (OG) detergent monomers distributed inside explicit solvent cell. In addition, the diffusion coefficients of the ligands (OG, $Ca^{2+}$, $Mn^{2+}$, and $Cl^{-}$) and the water molecules were also reported. The structural flexibility of the lectin was conserved in all simulations. The self-assembly of OG monomers into a small micelle at the hydrophobic site of the lectin was noticed in the simulation with 20 OG monomers. The interaction energy analysis concludes that the lectin was appropriately termed an adaptive structure. One or rarely two binding sites were observed at an instant in each simulation that were electrostatically favoured for the OG to interact with the surface amino acid residues. Enhanced binding of OG to the pea lectin was quantified in the system containing only $Ca^{2+}$ divalent ions. Interestingly, no binding was observed in the simulation without divalent ions. Furthermore, the lectin–ligand complex was stabilized by multiple hydrogen bonds and at least one water bridge. Finally, the work was also in accordance with the published work elsewhere that the simulations performed with different initial conditions and using higher nonbonded cutoffs for the van der Waals and electrostatic interactions provide more accurate information and clues than the single large simulation of the biomolecular system of interest.


*Keywords:* Octyl-glucopyranoside; Ligand binding; Pea lectin; Lipid self-assembly; Interaction energy; Diffusion coefficient

## 1. Introduction

Initially lectins were defined as agglutinins that could selectively agglutinate red blood cells based on their blood group type[1,2]. Today the term is widespread and frequently found in studies of protein–carbohydrate interactions [3–6] as a tool to probe the number and distribution of saccharide units, and to tag cells via glycoconjugates on the surface of the cell membrane [7,8]. Reports have also shown that some lectins bind to glycoprotein receptors on the lymphocyte cells, stimulating mitogenesis [9]. The legume lectin studied in this work is a pea lectin, a mitogenic globular protein isolated from the seeds of garden pea (*Pisum sativum*) by affinity chromatography [9–11]. Though the structure of the pea lectin shows very close resemblance to other leguminous lectins like Con A, lentil, and broadbean, their binding specificity and affinity toward carbohydrate derivatives are different for each [12]. At neutral pH, pea lectin exists as a dimer of one pair of α-chains, each 6000 Da, and one pair of β-chains, each 18,000 Da, whereas Con A, the only lectin among these legume lectins, exists as a tetramer.

Most lectins reported in the literature are categorized as carbohydrate binding proteins of non-immune origin that bind glycolipids and glycoproteins on the cell surface [4,12]. To observe the binding affinity and biological activity of the lectins, $Ca^{2+}$ and $Mn^{2+}$ divalent metal ions are envisaged for the binding or docking of sugar residues onto the protein surface. The three-dimensional crystal structure of the majority of these lectins, in particular from the legume family (isolated from

* Corresponding author. Institute of Thermodynamics, Helmut-Schmidt-University / University of the Federal Armed Forces Hamburg, Holstenhofweg 85, D-22043 Hamburg, Germany. Tel.: +49 40 6541 3500; fax: +49 40 6541 2008.
*E-mail address:* Bernd.Niemeyer@hsu-hh.de (B. Niemeyer).

0301-4622/$ - see front matter © 2007 Elsevier B.V. All rights reserved.
doi:10.1016/j.bpc.2007.04.006

leguminous plants), are already deposited in the protein data bank (PDB). A large collection of these biological macromolecular structures, including proteins and nucleic acids deposited in the PDB to date, are derived from either X-ray crystallography or NMR analyses. The latter method also provides some detail about the dynamics of the macromolecular complex in solution. Despite the increasing number of known structures, determining the structural and dynamic properties of a macromolecule experimentally and/or theoretically remains a challenging endeavor. The X-ray crystal structure of pea lectin has been determined at 6 Å [10] and 3 Å [11] resolutions. In addition, pea lectin complexed with D-glucopyranose has been reported and the atomic coordinates derived from an X-diffraction experiment at 1.9 Å resolution have been deposited in the PDB (entry code 2BQP) [13]. The diffraction results reveal that the coordination of $Ca^{2+}$ and $Mn^{2+}$ metal ions in the protein–carbohydrate complex is formed by ion–dipole interactions among four water molecules and six amino acid residues (Glu-119, Asp-121, Phe-123, Asn-125, Asp-129, and His-136). The D-glucopyranose binding site is stabilized by six hydrogen bonds (Asp-81, Gly-99, Asn-125, Ala-217, and Glu-218) located at the surface of the lectin monomer, in a shallow depression [13]. The van der Waals contact with the side chains of Phe-123 and Ala-80 residues additionally stabilizes the carbohydrate binding.

The carbohydrate ligand used in this work is an *n*-octyl-β-D-glucopyranoside (OG) molecule with a glucose head and a small octyl hydrocarbon tail [14,15]. This is a nonionic glycolipid used largely for the solubilization and crystallization of membrane proteins [16]. The main advantage of using an OG for such studies is that it has a high critical micelle concentration and low molecular weight and thus forms small spherical/ellipsoidal micelles in the solution that can be easily separated by dialysis. Considered mild detergent, OG can be easily handled at higher concentrations for the solubilization of proteins without denaturation of their function. They have several additional important characteristics: they can be synthesized on a large scale from renewable resources and are nontoxic and biodegradable. The carbohydrate ligands that bind to the lectin are more flexible in nature and exhibit larger dynamics in solution. This complexity deters experimental measurements in spite of advances in early kinetic experiments (titration calorimetry [12] and microcalorimetry [17]) and later diffraction and spectroscopic experiments [3] for the binding interaction analysis of carbohydrate–lectin systems at the molecular level.

A few factors in this regard that complicate experiments are the dynamic nature of active binding sites [5,18], quantitative measures of various forces involved in such bindings, specific affinity calculations of individual molecules in a complex in terms of binding free energies [19–23], instantaneous hydrogen bond formation and disruption between the molecular complexes, screening of electrostatic interactions [24], and the effect of explicit water on the complex formed [25,26]. Reviewing the facts, the present work outlines more accurate molecular dynamics (MD) simulations performed on pea lectin with different concentrations of OG molecules in an explicit solvent environment. These methods have been very successful for studying the structure, dynamics, and energetic properties of bimolecular systems [27,28]. Published results on the DNA–*Eco*RI biomolecular complex employing MD simulations in a 7.0 Å solvent shell indicate that the nonspecific interactions (i.e., between the DNA backbone and protein) were stronger than the specific interactions (i.e., between the DNA base and protein) [26]. The DNA and the protein were highly correlated with tight binding between the molecular entities. The presence of water bridges further increases the overall stability of the complex. Another report on Con A lectin with different saccharide substrates shows a favourable interaction with trimannoside (Man-α-(1→6)-[Man-α-(1→3)]-Man) compared to pentasaccharide (β-GlcNAc-(1→2)-α-Man-(1→3)-[β-GlcNAc-(1→2)-α-Man-(1→6)]-Man) [4]. The magnitude of the relative binding free energy is much higher in trimannoside than pentasaccharide substrates. The reduced binding in pentasaccharide has been found to be a result of significant distortion in the structure with an incomplete offset of the substrate and lectin desolvation from poor polar interactions [4].

To the best of our knowledge, the first to study the properties of pea lectin with MD simulations, we have made an effort to run the simulations in a realistic manner. Ten different models revealed the structure, interactions, and dynamic properties of the pea lectin accompanied with OG ligand at different concentrations in aqueous solution (see Table 1). Previous experiments have reported the importance of $Ca^{2+}$ and $Mn^{2+}$ metal ions for the biological activity of the lectin–ligand complex [11,13], in order to verify this effect the bivalent ions were completely removed from the equilibrated solvent box in one MD

Table 1
Description of the different MD simulations performed in this work with pea lectin, OG monomers and charged ions

| Simulation | System size (no. of atoms) | Model components | OG concentration (M) | Simulation model details |
|---|---|---|---|---|
| MD1 | 60,231 | 20 bog[a], 10 ca[b], 10 mn[c], 33 cl[d] | 0.059 | 20 OG monomers |
| MD2 | 59,961 | 10 bog, 10 ca, 10 mn, 33 cl | 0.029 | MD2 and MD3: 10 OG; |
| MD3 | 59,886 | 10 bog, 10 ca, 10 mn, 33 cl | 0.029 | different initial conditions |
| MD4 | 60,030 | 10 bog, 10 ca, 13 cl | 0.029 | No manganese ions |
| MD5 | 59,865 | 10 bog, 10 mn, 13 cl | 0.029 | No calcium ions |
| MD6 | 59,965 | 10 bog | 0.029 | Only OG monomers |
| MD7 | 59,805 | 5 bog, 5 ca, 5 mn, 13 cl | 0.015 | MD7 and MD8: 5 OG; |
| MD8 | 59,790 | 5 bog, 5 ca, 5 mn, 13 cl | 0.015 | Different initial conditions |
| MD9 | 59,748 | 2 bog, 2 ca, 2 mn, 1 cl | 0.0059 | MD9 and MD10: 2 OG; |
| MD10 | 59,700 | 2 bog, 2 ca, 2 mn, 1 cl | 0.0059 | Different initial conditions |

[a] *n*-octyl-β-D-glucopyranoside (OG).
[b] $Ca^{2+}$divalent ions.
[c] $Mn^{2+}$divalent ions.
[d] $Cl^{-}$ monovalent ions.

simulation (MD6, Table 1). The outlined specific structural and interaction analysis of the pea lectin with OG will improve our understanding of the complex interactions at the molecular level. The theoretical knowledge derived can also be helpful for studying and understanding the properties of other proteins incorporated on the surface cell membrane employing glycolipid detergents.

## 2. Methods

### 2.1. Lectin structure preparation

The crystal structure of carbohydrate binding pea lectin (2BQP) determined from X-ray diffraction was used as an initial structure for the MD simulations with explicit solvent [13]. Only the structural coordinates of pea lectin reported from the diffraction experiments were used in the present MD simulations. The OG ligands and metal ions were added separately into the solvent cell (Fig. 1). Simulation of such large protein structures using periodic boundary setup requires a large number of solvent molecules to treat the protein in an appropriate manner, which leads in computations to exponential growth. Because of this and also because the two subunits showed striking resemblances in their structures, only one subunit was considered for the all-atom MD simulations [10,11]. The PDB structure has a disordered loop of six missing residues (Asn-182–Glu-187) in the subunit chain. The missing residues were covered by the offset command in the CHARMM (Chemistry at HARvard Macromolecular Mechanics) program [29]. The histidine residues in the crystal structure of pea lectin were protonated at the NE2 atom for the MD calculations. Because the experimental pH of the lectin was 7.0, the addition of the proton to the histidine residues allowed the correct determination of the protonation state in the simulation. The hydrogen atoms were initialized and rebuilt with the CHARMM hbuild utility. An amino acid sequence of 228 residues with two chains (β-chain: 1–181 and α-chain: 182–228) was present in the final structure and the coordinates of the pea lectin molecule were saved to the CHARMM Cartesian Coordinate format.

Prior to the treatment of the lectin structure with an explicit solvent it was minimized in the vacuum state to reduce high potential energy barriers inside the structure. Harmonic constraint with a high force constant of 20 kcal/mol was used initially to hold atoms together tightly, then the structure was minimized with the 100 steps of Steepest Descent (SD) minimization method. The energies reported in this study are in kcal/mol because CHARMM utilizes this system of energy units for MD computations [29]. The computed energies can be readily converted to SI units as 1 kcal/mol=4186 J/mol. In addition, several parameters applied during model building and in simulations were in non SI units and thus followed the same procedure to compare the results directly with the other MD theoretical works. The minimized coordinates were correlated with the comparison sets and the structure was oriented based on root mean square difference for further relaxations. Subsequently force constants of 10 kcal/mol, 5 kcal/mol, and, at the end, no harmonic constraints were used with the minimization of 50 steps of Adopted Basis Newton Raphson (ABNR) and 200 steps of SD methods, respectively, before the lectin was completely removed from the constraint (freed lectin) [30].

### 2.2. Solvated lectin and glycolipid molecules

A tetragonal (TETR) periodic cell of 90×90×75 Å was constructed separately for the water molecules with the TIP3P model potentials [31]. The initial box contained 19,998 water residues and was subjected to 200 steps of SD and 400 steps of ABNR minimizations to relieve bad contact between the residues. Relaxation of the bulk solvent box was performed in the NPT ensemble along with other nonbonded options (see next section) for 25 ps of heating and equilibration stage each. Following the equilibration of the solvent cell a 14 Å hole was made at the center of the cell to place the lectin monomer inside. Water molecules approximately 2.0 Å from

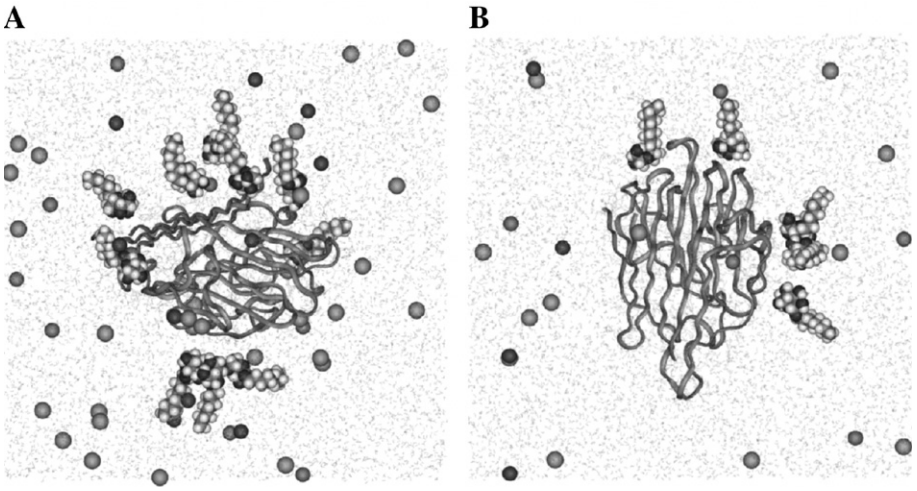


Fig. 1. Initial simulation models for the pea lectin with (A) 10 OG and (B) 5 OG monomers in the periodic tetragonal solvent cell. The lectin at the center is represented as backbone secondary ribbon, OG (van der Waals spheres), $Ca^{2+}$, $Mn^{2+}$, and $Cl^{-}$ ions as van der Waals atomic spheres distributed in the solution and the water molecules are made transparent for the clarity.

the lectin were removed after the lectin monomer was placed at the center.

The OG lipid molecules were generated independently in this study. Langevin dynamics simulations were carried out for the OG monomer for 1 ns and the random monomer conformations were stored for every 1000 ps [30]. Different conformations of the OG were selected randomly from the trajectories produced and distributed around the pea lectin monomer. Keeping the lectin monomer at the center, different numbers of glycolipid molecules were added to simulations as listed in Table 1. The OG monomers were first translated from the center and then rotated around the lectin, facing the lipid head group near the lectin surface (Fig. 1). Solvent molecules closer than 1.0 Å from the OG monomers were deleted. The OG monomers and the lectin were initially constrained at their respective positions and the water molecules were allowed to move around the constrained segments with 200 steps of SD. The fixed segments were later unconstrained followed by 300, and 200 steps of SD and ABNR minimization methods. Finally, depending on the simulations performed, several divalent $Ca^{2+}$ and $Mn^{2+}$ ions were added to the system (Table 1) for biological activity of the lectin macromolecule as determined from the experiments [11,13]. Water residues were randomly replaced by the ions and the ions were distributed such that none were closer than 3.0 Å to any of the molecular segments used in the model. The lectin molecule was again constrained for 200 steps of SD; the whole system was then freed from the constraints with 150 steps of SD and 200 steps of ABNR energy minimizations.

### 2.3. Details of MD computations

The MD simulations and analysis of the dynamic trajectories were performed with the program CHARMM version c30b1 [29]. The standard CHARMM potential energy surface function and parameter sets [32] were used in the computations together with other compatible force field parameters for the ligand molecules [33–36]. The complete model contains seven segments (two water segments, one pea lectin, OG, calcium, manganese, and chloride segments each). The number of OG monomers was varied from 20, 10, 5, and 2 monomers, respectively, in the MD simulations in addition to divalent ions as shown in Table 1. On average the total number of atoms in each simulation totaled ~60,000, with 3499 atoms for the pea lectin was common to all simulations. An equivalent number of anionic $Cl^-$ ions (Table 1) were also added to the TETR cell to keep the overall electrical charge of the cell neutral.

Hydrogen atom bond lengths in the simulations were constrained with the SHAKE algorithm [37]. The long-range nonbonded Lennard–Jones interactions between atom pairs were truncated at 14 Å. The cutoff scheme was handled by a force switch option from 10 Å to 14 Å. The nonbonded interaction pair lists were updated automatically when an atom in the current position moved by more than 1 Å. The electrostatic interactions were evaluated from a smooth Particle–Mesh–Ewald implementation using a grid size of 96, 96, and 80 points in all three directions [38]. The width of the Gaussian distribution kappa, $k=0.34$ Å$^{-1}$, was applied with the real space cutoff of 14 Å. With all these nonbonded options and image specifications, each final system was again minimized for 500 steps of SD and ABNR methods prior to the heating step. The integration time step of 2 fs was employed in the simulations. The atoms in the system were assigned an initial velocity according to the Maxwellian distribution from 0 K to 298.15 K over a 40 ps heating stage in the NPT (constant number, pressure, and temperature) ensemble [14]. During the equilibration stage the pressure inside the system was maintained at 1 atm with a pressure piston mass of 3000 amu and a Langevin piston collision frequency of 25 ps$^{-1}$. A Hoover thermostat with a thermal piston mass of 20,000 nnkcal ps$^2$ was applied to control the temperature of the system at 298.15 K [39]. Different initial coordinates and velocities were assigned to the simulations prior to the heating and equilibration, giving an excellent scope for the characterization of the molecular components in the simulations in an explicit solvent environment. All the simulations (10 MD runs) carried out from different initial conditions were extended for one nanosecond time scale. The properties reported from these systems are much more effective than a single long MD simulation [27].

### 2.4. Force field parameters and structural analysis

The energy minimized crystal structure of pea lectin was applied with CHARMM22 force field parameters [32]. The partial charges of the OG were taken from the Carbohydrate Solution Force Field (CSFF) and appended to the lectin topology and parameter file [33–35]. The manganese and chloride ions parameters used in the simulations are derived from free energy simulations [40]. The charges and van der Waals parameters chosen for the divalent cations were, for calcium, $q=+2$, $\varepsilon$ (kcal/mol)$=-0.12$, and $R_{min}/2$ (Å)$=1.71$ and, for manganese, $q=+2$, $\varepsilon$ (kcal/mol)$=-0.015$, and $R_{min}/2$ (Å)$=1.185$. For the chloride anion these parameters were $q=-1$, $\varepsilon$ (kcal/mol)$=-0.15$, and $R_{min}/2$ (Å)$=2.27$. The structural conformations of the lectin simulations were evaluated by root mean square (RMS) deviations of the solvated lectin against the initial crystal structure with respect to the simulation time. Positional fluctuations of the lectin atoms were calculated for the backbone and side chain atoms on the basis of differences in the average solution structure of the residue. These calculations gave an estimate of the stability and fluctuations of the lectin structures in solution as a function of their atomic positions. The lectin backbone RMS fluctuations were (RMSF) compared with the X-ray crystallographic structure through the Temperature-or B-factor parameter with a simple correlation ($B=[8/3\ \pi^2<RMSF^2>]$) that reflects the underlying fluctuation of atoms about their average position and measures the important dynamics involved in the amino acid residues of the proteins [41,42]. Furthermore the solvent-accessible surface areas, hydrogen bonding analyses, and diffusion coefficients for all molecular components in the simulations were analyzed thoroughly and also compared to the available experimental and theoretical works reported in the literature. The computations were performed on an HP parallel computer with 64-bit Intel Itanium2 processor and took several months of computation time because of the very large size of the

system and the higher cut-offs of the nonbonded interactions in an explicit solvent periodic cell. The dynamic trajectories were analyzed partly on the HP/Intel Itanium2 and SGI Octane2 workstations.

## 3. Results and discussion

### *3.1. Flexibility and dynamics of lectin structural conformations*

Flexible regions in the three-dimensional structure of the globular proteins have customarily been judged by the RMS deviations of the backbone and side chain atom coordinates in the MD simulations with reference to the crystal structure [41,43]. Despite the fact that the simulations started from different initial conditions, concentrations of OG, number of ions, and solvent molecules the global conformations of the lectin fairly converged to the stable state as shown in Fig. 2A and B. The correlations of protein structures between different simulations improved significantly as the simulation proceeded to the nanosecond range. This suggests the protein structures in the solution were in an equilibration state. Higher molecular fluctuations were observed in the MD9 simulation consisting of two OG monomers in the TETR cell. At greater than 0.5 ns the deviations in this system were slightly higher than in the other simulations but as it proceeded the lectin relaxed in the solvent and slowly approached a decreasing plateau toward the end of the run (MD9 in Fig. 2B). The exact reason for this temporary deviation was not known but we suggest that the lack of sufficient divalent ions in this simulation might have caused the lectin to fluctuate more before stabilizing the structure in the solution. Kumar and Nussinov have shown that close-range electrostatic interactions tend to shift the equilibrium point toward the native state and to constrain backbone flexibility [24]. However, the presence of side-chain atoms in the globular proteins seems to promote fluctuations in responses to the surrounding environment [25].

The individual backbone conformations of the lectin from the equilibrium MD simulations are shown in Fig. 3 in a wire representation along with the superimposed starting crystal structure. An analysis of MD trajectories for the average residue RMS deviations in solution shows that the backbone atoms were more stabilized and fluctuated little in the solution. The pea lectin monomer was separated into several molecular components in the following order: whole monomer, monomer

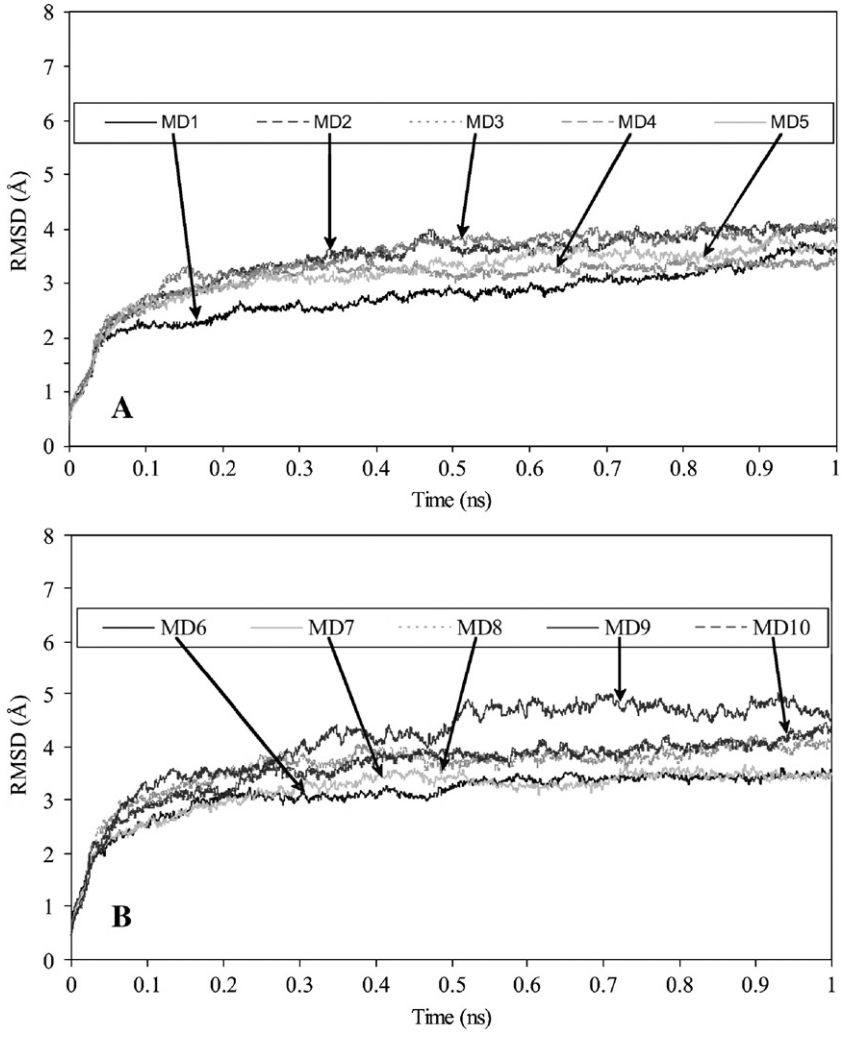


Fig. 2. Time evolution of the RMS deviations of the pea lectin heavy atoms in the simulations. (A) MD1–MD5 simulations, (B) MD6–MD10 simulations.

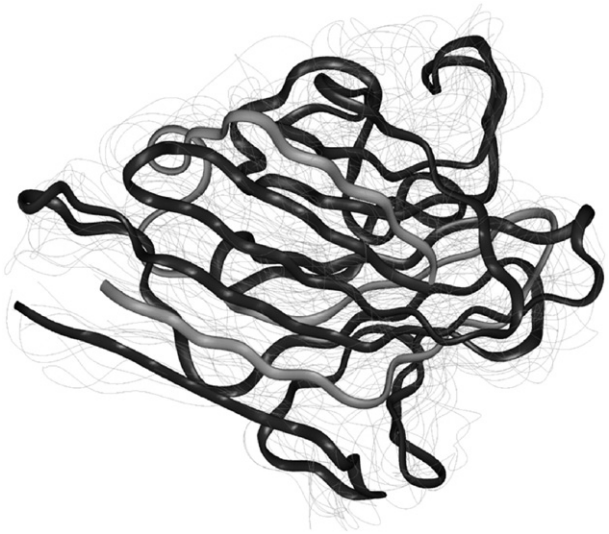

Fig. 3. MD averaged flexible lectin conformers from the simulations shown as wires (grey) are compared with the superimposed initial crystal structure (solid ribbon). All other molecular components were blanked (refer Fig. 1).

backbone, monomer side chains, β-chain, β-backbone, β-side chains, α-chain, α-backbone, and α-side chains. The results for the RMS deviation are not shown but the same terminology is followed in the other parts of this report wherever necessary. The average residue RMS deviations calculated for the MD9 simulation exhibited higher conformational change in the monomer β-chain residues of Thr-57, Lys-93, Gln-114, Trp-128, and Asn-132. These residues are mainly uncharged polar groups and have longer side chains that fluctuate with the surrounding medium. Moreover, the size of the lectin calculated from the radius of gyration was not changed in the simulations over time. The constant size was attained in the early stage of the simulation and maintained steadily for the rest of the simulation. This indicates that the conformational shape change observed in the MD9 was only local [26].

The internal atomic motions of the pea lectin in the simulations were characterized by the RMS fluctuations averaged per residue around the average solution structure. The average RMS fluctuation in each simulation is estimated for the lectin heavy atoms, backbone atoms, and side chain atoms. Averages from the independent runs show that the lectin backbone in the simulations was closer to the average solution structure with smaller fluctuations than the lectin side chains (figure not shown). In addition, the fluctuations were symmetric in all simulations, with a slightly higher deviation in the MD9 simulation. It was known from the above RMS deviations that the structure in this simulation would be more flexible and exhibit larger conformational fluctuations in solution; however, these fluctuations are quite acceptable for dealing with such large systems [22,25]. As a result of thermal motion of the atoms in the globular proteins the molecular components were constantly moving in the solution. The B-factor distribution was calculated to quantify the amino acid residues in the protein structure leading to larger dynamics. The B-factor determined from the MD simulations was calculated from the RMS fluctuations of the backbone atoms of the lectin [26,41] and compared to the experimental results [13]. Analysis of the B-factor provides important information about protein dynamics [42]. It is also used in a variety of applications, such as predicting protein flexibility and thermal stability, analyzing active sites, and investigating protein disordered regions [4,42]. In Fig. 4 the B-factor results from the crystallographic structure and the MD simulations performed in the solution phase for 20, 10, 5, and 2 OG monomers are compared. The important conclusion from this analysis is that the larger dynamics observed in the X-ray crystal structure were also retained in the lectin simulations carried out in the solution phase. However, larger dynamics were observed in the solutions because of the additional nonbonded (electrostatic and van der Waals) interaction forces from the surrounding environment and hydrogen bonding of the surface residues in the pea lectin with the OG and water molecules. These nonbonded interactions and

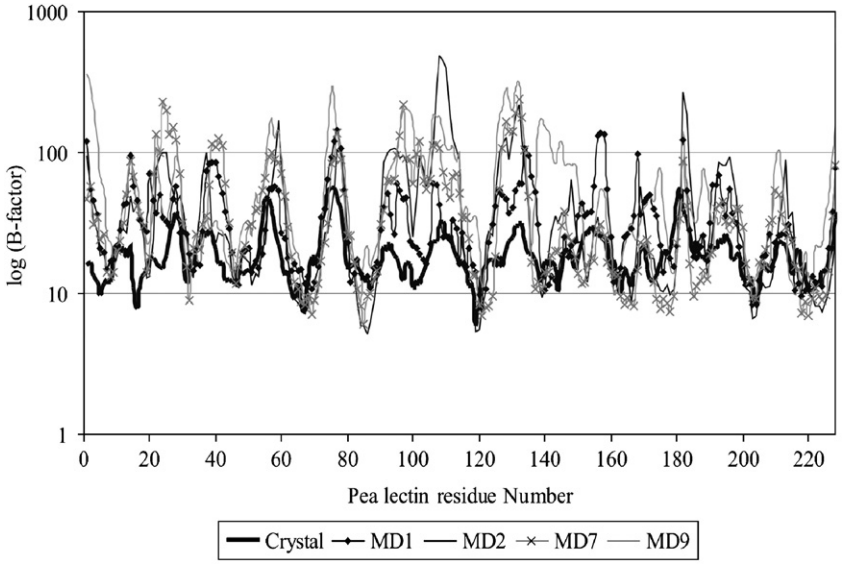


Fig. 4. Lectin residue dynamics computed from the B-factors are compared between X-ray crystallographic data and the MD simulations performed with 20 (MD1), 10 (MD2), 5 (MD7) and 2 (MD9) OG monomers.

hydrogen bonding networks are crucial for the stability and flexible movement of specific residues in the lectin [24]. The overall B-factor determined from the crystallization experiments was 20.4, which is smaller than the values calculated from the average backbone RMS fluctuations in the MD simulations (table not shown). The average B-factor value from these simulations was 34.1 for the pea lectin.

Interestingly, most of the peaks found in the experimental B-factor profile are well matched with the MD simulations except at a few locations in the residues sequence from Pro-12 to Ile-19 and Lys-92 to Tyr-109 (Fig. 4). The experimental B-factor is not well characterized at these regions because of a lack of motion in the crystal structure in contrast to the free all-atom explicit solvent MD simulations. It is known that proline is a cyclic residue that is most often involved in the turn regions of the β-pleated sheet similar to the region observed in the pea lectin. The latter region (Lys-92 to Tyr-109) is located at the surface of the globular protein in a shallow indent that provides a place for the solvent or OG molecules to interact with it effectively. In addition, the 4-aminobutyl side chain of Lys-92 and the three-carbon cyclic chain of Pro-93 induce further dynamics at these regions that were not captured correctly in the experimental measurements.

### 3.2. Surface characterization of the pea lectin monomer

The evolution of conformational changes on the lectin surface near the solvent environment plays a fundamental role in the hydration of side chains of the hydrophilic amino acids in most of the globular proteins. As expected the simulations that started from the minimized crystal structure increased at the early stage of the simulation because of the conformational relaxations in the solution. Once the lectin surface was stabilized by providing a constantly accessible surface to the solvent molecules, an increase in solvent-accessible surface area was not observed in the simulations (figures not shown). The α-chain of a pea lectin in the simulations reached equilibrium state much more quickly than the β-chain. Unlike the β-side chains, the β-backbone seems to be in good correlation with the molecular components of the α-chain. The only group requiring more equilibration than the other components in the lectin monomer was the β-side chains. After ~500 ps the β-side chains in the solution also reached an equilibrium condition. Because of the higher number of residues in the β-chain (approximately four times larger in size) equilibration took longer than for the α-chain entities [26].

The total solvent-accessible surface area (SASA) of the pea lectin in the solution from the simulations is listed in the Table 2. In spite of the increase in SASA from the time-averaged solution trajectories, good agreement of the results was obtained with the X-ray diffraction crystal structure. The average SASA of the ten simulations calculated with the probe radius of 1.6 Å was $11.2 \times 10^3$ Å$^2$ [44]. This value is comparable to $9.2 \times 10^3$ Å$^2$ per pea lectin monomer reported by Pletnev et al. with a similar probe size of 1.6 Å [13]. The relative contributions from each molecular component to the total pea lectin monomer were also analyzed and listed in Table 2. These results

Table 2
Percentage contribution of lectin chains to the solvent accessible surface areas

| MD simulation | Total ($10^3$ A$^2$) | β-chain (%) | β-side (%) | β-back (%) | α-chain (%) | α-side (%) | α-back (%) |
|---|---|---|---|---|---|---|---|
| MD1 | 10.84 | 83.57 | 74.21 | 9.35 | 16.43 | 14.03 | 2.41 |
| MD2 | 11.25 | 83.21 | 72.30 | 10.91 | 16.79 | 14.60 | 2.19 |
| MD3 | 11.15 | 83.73 | 73.07 | 10.65 | 16.27 | 14.17 | 2.11 |
| MD4 | 11.01 | 84.33 | 73.84 | 10.48 | 15.67 | 14.04 | 1.64 |
| MD5 | 11.17 | 83.56 | 73.12 | 10.44 | 16.44 | 13.96 | 2.48 |
| MD6 | 10.73 | 83.67 | 73.42 | 10.25 | 16.33 | 14.15 | 2.18 |
| MD7 | 11.54 | 83.63 | 73.34 | 10.29 | 16.37 | 14.54 | 1.84 |
| MD8 | 11.21 | 84.71 | 72.75 | 11.95 | 15.29 | 13.24 | 2.05 |
| MD9 | 12.20 | 82.54 | 71.44 | 11.10 | 17.46 | 15.05 | 2.41 |
| MD10 | 11.34 | 84.19 | 73.50 | 10.69 | 15.81 | 13.97 | 1.83 |

show that more than 80% of the SASA are from the β-chain, which is indeed from the amino acid β-side chains. Only about 16% was contributed by the α-chain to the total monomer SASA. In addition, higher interactions of solvent molecules with the β-backbone (MD8 and MD9) and α-side chains (MD9) are noted in Table 2 from these simulations compared to the other MD runs. The β-backbone in these structures was more dispersed in the solution and thus in direct contact with the solvent molecules. This might be the result of more fluctuations observed in the MD9 simulation (Fig. 2). In contrast to these results a very different view has been reported by Wriggers et al. [41]. Their MD simulation with the calcium-sensing calmodulin protein exhibits a decrease in SASA against the crystal structure. In addition, the authors examined the decrease in SASA's in the crystal and solution structure of calmodulin as probe radius increased from 1.4 Å to 20 Å [41]. These studies are useful for a rough estimate of the protein aggregate surface but will not provide details of specific interactions between the protein–ligand complex and the hydrogen bonding/water bridge patterns involved in the active binding site of the protein.

### 3.3. Glycolipid–protein interaction energies

To quantify the specificity of the recognition/binding of OG monomer to the amino acid residues in the lectin, interaction energies between OG and the lectin monomer were analyzed for the different systems simulated (Fig. 5). The nonbonded electrostatic (black) and van der Waals (dark grey) terms contributing to the total interaction energy are shown in Fig. 5A, B and C from the 20, 10, and 5 OG monomer simulations, respectively. It is clearly seen from these profiles that one or rarely two OG monomers in the simulations interact with the lectin monomer on a specific site location. The most specific interaction of MD1 comes from OG-8 and OG-16 monomers, whereas for the MD2 it is OG-6 and rarely OG-7. The OG-3 monomer interacts strongly in the MD7 simulation. Electrostatic interaction plays a very important role in all of these simulations, contributing significantly more to the total interaction energy (light grey) than the van der Waals interactions [24,25,45]. Moreover, the latter interactions have also been observed in these simulations and they actually stabilize the lectin monomer further.

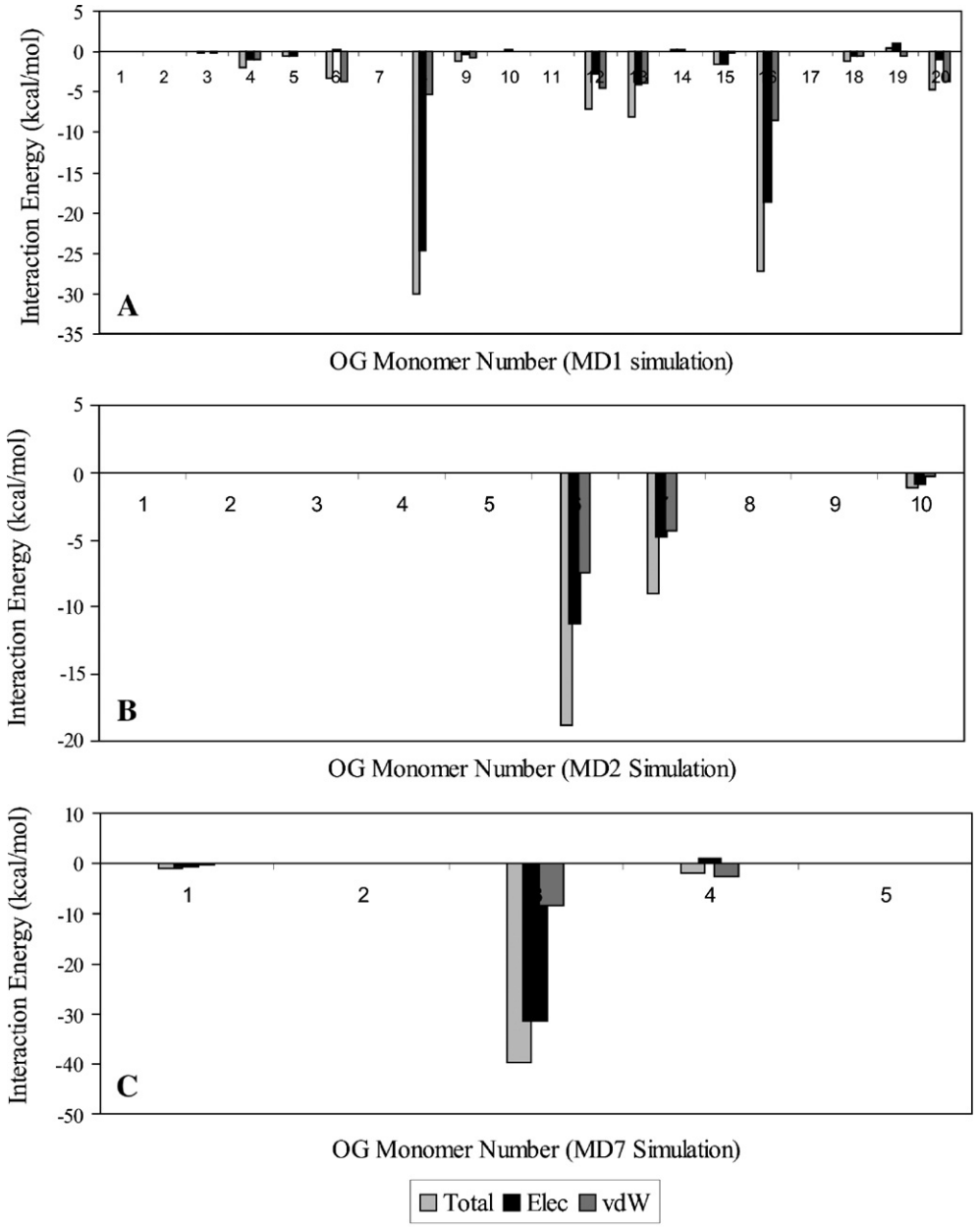


Fig. 5. Total interaction energies (light gray line), electrostatic (black line) and van der Waals (dark grey line) energy contributions for each OG monomer with the pea lectin from MD1 (20 OG monomers), MD2 (10 OG monomers), and MD7 (5 OG monomers) simulations.

Detailed analysis of the OG binding on the specific site was carried out to check the forces involved in making some of the residues in the protein more favourable for the interactions. As observed in the stability analysis, the addition of various concentrations of OG in the simulations did not disturb the overall conformation of the lectin in solution. It has to be kept in mind that the detergent concentration used in this work was very low, close to the critical micelle concentration. Higher concentrations of OG might have an influence on the structure of the lectin; this might be the subject of another detailed study. Abundant research has been carried out over decades on the usage of OG as a detergent for the crystallization and solubilization of proteins [16,46,47]. These studies conclude that the short-chain glycolipids were more successful than the longer chains because they fit around the hydrophobic regions without disturbing the hydrophilic inter-residue interactions [48]. Thus we expect the hydrocarbon chain in OG is also small and the addition of these monomers will not hinder the flexibility of the lectin. Our perspective is in fact in good agreement with the interaction studies performed on melittin protein with different detergents by Lauterwein et al. using a broad range of physicochemical methods where it was concluded that interactions with detergents were similar to those in a phospholipid bilayer environment [49]. With this past and present knowledge we are assured that the interaction of OG with pea lectin will preserve the lectin in a native state. As shown in Fig. 5A the interaction of OG-16 with the lectin was stable throughout the trajectories analyzed. The detergent head group interacted

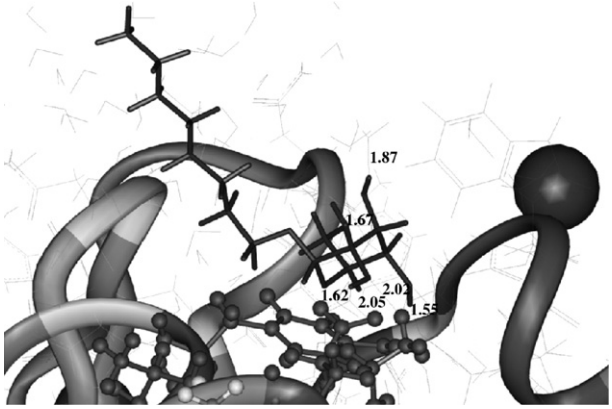


Fig. 6. Close stereo view of the OG monomer (represented as black sticks) around the lectin (ribbon) binding site. The OG monomer is stabilized by the $Ca^{2+}$ divalent ion (dark van der Waals atomic sphere) next to the binding site. The light grey colors marked on the ribbon diagram of the lectin are the residues involved in the binding site reported from the X-ray diffraction study [13]. The favourable interacting side chain lectin residues with the OG monomer in the MD simulation are shown in a ball and stick representation.

strongly with the lectin residues Tyr-100, Leu-101, Ala-107, Glu-108, and Lys-145. As shown in Fig. 6 the binding site of OG-16 from the MD1 simulation in the solution was very close to the X-ray diffraction crystal structure [13]. The residues involved in the binding site of the glucose ligand in the crystal structure are marked light grey. Even though the ligand used in the MD simulation is a glycolipid with an octyl hydrocarbon tail, the binding site of the glucose head group on the lectin surface was more or less similar to the glucose ligand determined from the crystal structure. In addition, similar to the observation in the crystal structure, the binding of the $Ca^{2+}$ ligand ion (shown as dark van der Waals sphere) on the lectin was also close to the OG-16 monomer in the solution simulation (Fig. 6).

A different binding mechanism has also been observed in the MD2 simulation in comparison to the MD1 simulation (Fig. 5B). The van der Waals energies involved in the interactions were relatively higher than the MD1 simulation, where electrostatic energies largely dominated. The two monomers (OG-6 and OG-7) in the simulation were lying completely on the lectin surface (Phe-6, Leu-7, Ile-8, and Leu-18 residues for OG-6 and Ile-8 and Lys-10 for OG-7) and shielding the hydrophobic residues with the OG monomers [16]. This must be the main cause of the increase of van der Waals energies for such bindings. The OG monomer tails interacted with these hydrophobic residues (particularly isoleucine) very strongly on the lectin surface without being released back into the solution. The interaction in the MD7 simulation is similar to the interactions in MD1 with a single OG-3 monomer interacting with the residues Asp-23, Val-41, Gln-95, and Gly-97 (Fig. 5C). The glucose head bound to the charged aspartic acid and glutamine residues and the octyl tail to the valine residue.

Another interesting event observed in the MD1 simulation was "micellization," a very practical mechanism commonly appearing with the detergents employed for the protein solubilization. The concentration of the OG in this simulation was at just above the critical micelle concentration so it was favoured to form a micelle with a small hydrocarbon core. Our previous experience with the OG and results in the literature indicate that OG aggregation numbers of 10 monomers or above are more stable in solution after the formation of small micelle aggregates [14,50]. The randomly dispersed OG monomers around the lectin at the beginning of the simulation (Fig. 7A) began to be self-assembled by the formation of a small micelle of ~10 monomers (Fig. 7B). As noticed from the dynamic trajectories and the interaction studies, the OG-13 monomer initially interacted with the charged residues of Lys-200 and Asp-201 by favourable electrostatic energies, whereas the OG-8 monomer interacted with the side chains of the highly hydrophobic Val-172, Leu-173, and Val-196 residues at the surface. With this OG-8 monomer bound tightly by strong hydrophobic interactions at the protein surface, it started slowly dragging the surrounding OG monomers and prevented solvent molecules from interacting with the lectin hydrophobic site. Thus the lectin surface residues provided a base for the aggregation of OG monomers. This preformed small aggregate interacted with the

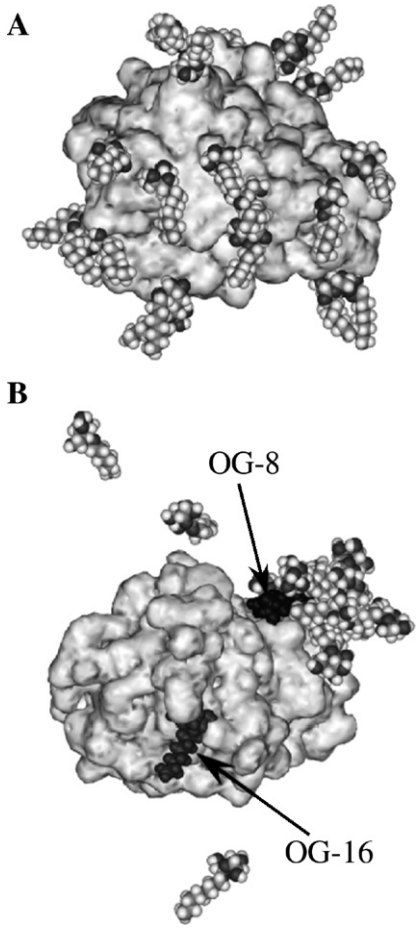


Fig. 7. The snapshot outlines the system with 20 OG (van der Waals spheres) monomers. The evenly distributed OG monomers at the start of the simulation (A) have evolved to a micelle aggregate (B) of about 10 OG monomers at the surface of the lectin (grey solid) with the OG-8 (black) monomer acting as a bridge between these two. Also the OG-16 monomer at the binding site on the lower part of the lectin was shown in dark grey.

other OG hydrocarbon tails and started to build the micelle with its strong hydrophobic core centered on the surface of the lectin's hydrophobic site (Fig. 7B). As a result of this hydrophobic effect OG-13 and nearby OG monomers in the solution were influenced by the screening of the hydrophobic forces from the newly created micelle. During this process the hydrophobic side chains of the lectin held the central part (most probably the acetal oxygen of the glucose head group) of the OG-8 monomer close to it with the OG head group pushed slightly inside the proton cloud of Thr-192 and Asp-195 residues, increasing electrostatic interactions with the lectin and the tail lying in the micellar core (OG-8 monomer colored black in Fig. 7). Thus in this case the OG-8 monomer acted as a bridge between the lectin and the micelle aggregate.

The monomer involved in the aggregation process was analyzed by the distance matrix averaged over the center of geometry of the hydrocarbon tails in the OG monomers. The distance was calculated for the OG monomers based on the center of geometry of the OG-8 monomer tail before and after the formation of the micelle. This analysis gives the trace of distance traveled by the OG monomers in the solution and compares it with the initial distances, shown in Table 3. The initial distances of the monomers from the reference OG-8 monomer are listed in the second column. The final distance shown in the third column of Table 3 was calculated from the last 400 ps dynamics trajectories and the distance values were averaged over the corresponding MD frames. The process of spontaneous micelle formation, which usually takes a longer simulation time, in the range of several nanoseconds [14], was observed very quickly in this study. This seems due to the presence of the lectin hydrophobic side chains at the surface and facilitates to some extent the rapid formation of the micelle. In addition to the individual lipid monomers interacting with the proteins [46,48], the formation of the micelle aggregate will also contribute to the solubilization process of the proteins.

The influence of divalent ions on the OG interaction with the lectin are presented in Fig. 8A, B and C showing the interaction energy profiles for the systems containing either $Ca^{2+}$ or $Mn^{2+}$ ions or neither of these ions (only OG monomers) in the MD4, MD5, and MD6 simulations. It is clear that the binding of OG monomers to the lectin was enhanced in the system containing $Ca^{2+}$ ions and OG (Fig. 8A). Several bindings of OG monomers (OG-5, OG-8, OG-9, and OG-10) are apparent in this simulation with significant electrostatic interactions to the lectin residues (see ordinate scale). An increase in the magnitude of the interaction strength of OG-8 was observed in addition to the enhanced binding of OG-5 monomer contributing favourable electrostatic interactions to the Gly-98, Gly-99, Leu-101, Thr-215, and Gly-216 residues (Fig. 8A). Evidently, the presence of only $Ca^{2+}$ ions in the simulation increases the binding of OG monomers and also indicates the importance of this divalent ion for the binding of ligand molecules with the lectin. The binding was also near the crystal structure binding site. In an excellent review, Clapham stated that multiple bindings can be found within the same protein, which acts as a buffer to simply bind the $Ca^{2+}$ ions as their concentration is increased [51]. However, in this specific case with the OG ligands there is no clear evidence to support such behaviour. This point is not yet proved or analyzed by other authors so it is speculative at this moment. A relatively smaller number of binding interactions as well as weak forces were engaged for the OG monomers with only $Mn^{2+}$ divalent ions (Fig. 8B). The OG-5 monomer is the only monomer that shows a larger magnitude of binding to the residues of Glu-108 and Trp-128. Finally, the MD6 simulation with only OG monomers (all ions were removed in this simulation) clearly shows no interaction at all (Fig. 8C). In contrary to the other systems, the simulation without ions shows a positive electrostatic energy and a high negative van der Waals interaction energy for the OG-9 monomer. The OG-9 hydrocarbon tail interacts with the Phe-11, Ser-12, and Pro-13 residues and is enhanced by the van der Waals forces. This is the only monomer that shows unfavourable electrostatic interaction and a large van der Waals interaction with the lectin. The interaction energies of other OG monomers with the pea lectin monomer are negligible. From these results we can conclude that carbohydrate binding to pea lectin is strongly dependent on divalent ions. Without these ions the binding of the ligand molecules on the lectin active site would not be possible.

Table 3
Initial and the final (averaged) distance from the center of geometry of the OG-8 tail with respect to the other OG monomer tails that participate in the micelle formation in MD1 simulation

| OG monomer no. | Initial distance (Å) | Final[a] distance (Å) |
|---|---|---|
| OG-3 | 11.9 | 11.3 |
| OG-8 | 3.6 | 3.8 |
| OG-9 | 50.5 | 10.9 |
| OG-10 | 16.7 | 11.9 |
| OG-12 | 18.2 | 10.9 |
| OG-13 | 50.9 | 19.9 |
| OG-15 | 27.5 | 8.8 |
| OG-18 | 30.6 | 11.1 |
| OG-20 | 13.3 | 7.2 |

[a] The final distance values are averaged from the last 400 ps dynamic trajectories.

### 3.4. Hydrogen bonding and water bridging between ligand–lectin complexes

The orientation of water molecules and the OG monomers next to the lectin monomer are influenced by the constantly changing intermolecular attractions between the proton donor and the electronegative acceptor atoms [5,25]. The hydrogen bond calculations within solvent molecules and with the other molecular segments (Table 1) produced an enormous amount of data because of the large number of water molecules. More than 90% of atoms in the model constitute solvent, thus only hydrogen bonding and water bridges between pea lectin and OG monomers with a lifetime >50 ps from the solution trajectories of 400 ps were listed in Table 4, for all simulations except MD9 and MD10. The high hydrogen bond occupancy observed from the hydroxyl atoms of OG-13 with the Asp-201 residue occurred in the early stage of the simulation. It was later disrupted by the formation of the micelle aggregate. As stated above, the strong hydrophobic effect concentrated on the

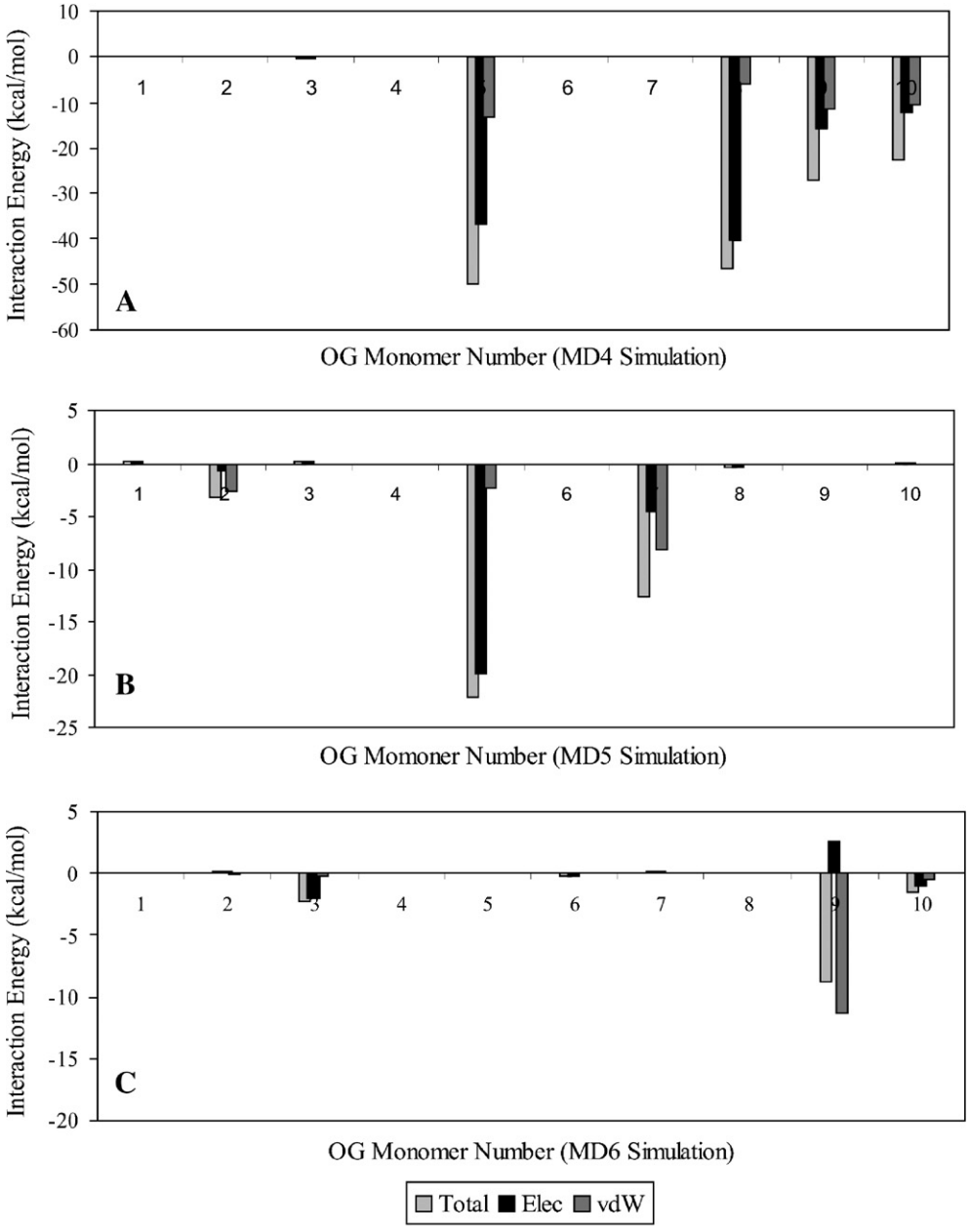


Fig. 8. Total interaction energies (light gray line), electrostatic (black line) and van der Waals (dark grey line) energy contributions for each OG monomer with the pea lectin from MD4 (10 OG and only $Ca^{2+}$ divalent ions), MD5 (10 OG and only $Mn^{2+}$ divalent ions), and MD6 (only 10 OG monomers, no ions) simulations.

lectin's hydrophobic site screened the surrounding OG molecules to diffuse into their hydrocarbon micellar core. After the aggregate was formed the OG-8 monomer took control of the hydrogen bonding mechanism from the micelle end with the strong attraction to the polar Asp-195 residue. The OG-16 monomer forms hydrogen bonds with three different charged residues (Glu-108, Asp-129, and Lys-145) in addition to a very stable water bridge with Tyr-100. The presence of this long-lived water bridge additionally stabilizes the protein–lipid complex [26]. The hydrogen bond fluctuations in this monomer seem to be higher than in the other monomers, which indicate that the binding site is more flexible and dynamic in nature. Continued sharing of intermolecular attractions between the hydroxyl atoms of the ligand and the charged residues of the lectin on the binding site might be the cause of short average hydrogen bond lifetime observed in the OG-16 monomer. Also, the longer side chain of Lys-145 residue at the active site moved more quickly in the solution, leading to disruption and reformation of hydrogen bonds. In spite of these fluctuations the ligand monomer is thermodynamically favourable at the shallow region of the carbohydrate binding site (Fig. 6 and dark grey in Fig. 7B).

In the MD2 simulation only OG-6 was involved in the hydrogen bonds with Phe-6 and Ile-8 residues; the same monomer was also occupied in a water bridge with Ile-8 residue. As seen, the hydroxyl atom of OG-6 formed a hydrogen bond with

Table 4
Important high occupancy hydrogen bonding and water bridges formed between pea lectin and OG monomers from MD simulations

| MD simulation | Lectin atoms | Ligand atoms | Average [a] lifetime (ps) |
|---|---|---|---|
| MD1 H-bond | (Lectin residues) | (20 OG monomers) | |
| | LEC:GLU-108:OE2 | HO2:16-OG:LIG | 90.0 |
| | LEC:ASP-129:OD1 | HO4:16-OG:LIG | 70.0 |
| | LEC:LYS-145:HZ2 | O2:16-OG:LIG | 65.0 |
| | LEC:ASP-195:OD1 | HO4:8-OG:LIG | 150.0 |
| | LEC:ASP-195:OD2 | HO4:8-OG:LIG | 97.5 |
| | LEC:ASP-201:OD1 | HO4:13-OG:LIG | 175.0 |
| | LEC:ASP-201:OD2 | HO3:13-OG:LIG | 135.0 |
| Water bridge | LEC:TYR-100:O | O4:16-OG:LIG | 220.0 |
| MD2 | (Lectin residues) | (10 OG monomers) | |
| H-bond | LEC:PHE-6:O | HO3:6-OG:LIG | 41.0 |
| | LEC:ILE-8:HN | O6:6-OG:LIG | 97.5 |
| | LEC:ILE-8:O | HO6:6-OG:LIG | 67.5 |
| Water bridge | LEC:ILE-8:O | HO6:6-OG:LIG | 50.0 |
| MD3 | (Lectin residues) | (10 OG monomers) | |
| H-bond | LEC:SER-190:OG | HO2:8-OG:LIG | 25.0 |
| | LEC:SER-226:HG1 | O4:4-OG:LIG | 35.0 |
| Water bridge | LEC:THR-65:OG1 | HO6:4-OG:LIG | 30.0 |
| MD4 | (Lectin residues) | (10 OG monomers) | |
| H-bond | LEC:ASN-17:HN | O2:10-OG:LIG | 93.7 |
| | LEC:LEU-18 :HN | O2:10-OG:LIG | 80.0 |
| | LEC:THR-96:OG1 | HO2:5-OG:LIG | 60.0 |
| | LEC:GLY-97:HN | O2:5-OG:LIG | 60.0 |
| | LEC:GLY-98:HN | O2:5-OG:LIG | 90.0 |
| | LEC:LYS-111:HZ1 | O2:8-OG:LIG | 70.0 |
| | LEC:THR-113:OG1 | HO6:8-OG:LIG | 230.0 |
| | LEC:THR-215:O | HO6:5-OG:LIG | 235.0 |
| Water bridge | LEC:ILE-8:O | HO4:10-OG:LIG | 60.0 |
| | LEC:THR-40:O | O4:5-OG:LIG | 85.0 |
| MD5 | (Lectin residues) | (10 OG monomers) | |
| H-bond | LEC:GLU-108:OE2 | HO2:5-OG:LIG | 60.0 |
| MD6 | (Lectin residues) | (10 OG monomers) | |
| H-bond | LEC:LYS-30:HN | O2:9-OG:LIG | 60.0 |
| MD7 | (Lectin residues) | (5 OG monomers) | |
| H-bond | LEC:ASP-23:OD1 | HO2:3-OG:LIG | 280.0 |
| | LEC:ASP-23 OD1 | HO3:3-OG:LIG | 80.0 |
| | LEC:GLY-42:HN | O2:3-OG:LIG | 82.5 |
| MD8 | (Lectin residues) | (5 OG monomers) | |
| Water bridge | LEC:ASN-78:HD21 | HO2:4-OG:LIG | 80.0 |
| | LEC:TYR-219:O | HO2:4-OG:LIG | 225.0 |

[a] The average lifetime was calculated from the last 400 ps dynamic trajectories.

Ile-8 residue directly and once it was broken, in some instances the interactions between these two atoms were still similar but interaction was stabilized through a water bridge. A relatively weak hydrogen bonding pattern has been observed in the MD3 simulation. Interestingly, in MD4 very strong hydrogen bonding and a couple of water bridges are apparent in the simulation with only $Ca^{2+}$ ions (no $Mn^{2+}$). Of three monomers involved in hydrogen bonding, OG-5, OG-8, and OG-10, the first two contribute largely to the hydrogen bonds. As seen in Table 4 (MD4) the HO6 donor atoms of the ligand are forming hydrogen bonds with the O and OG1 acceptor atoms of Thr-113 and Thr-215. These results state that the presence of $Ca^{2+}$ ions improves the hydrogen bonding pattern between OG and the lectin monomer. Reduction in the hydrogen bonding pattern was seen in the MD5 simulation with only $Mn^{2+}$ (without $Ca^{2+}$) ions. The HO2 of OG-5 created a hydrogen bond with the acidic Glu-108 residue in the MD5 simulation. The average lifetime of the hydrogen bond has been lowered in this simulation without the presence of $Ca^{2+}$ ions. Analyzing the results of MD6 indicate that the strength of the hydrogen bonding is decreased to a great extent with only OG monomers (without $Ca^{2+}$ and $Mn^{2+}$ ions). The negatively charged Lys-30 residue forms a hydrogen bond with the oxygen acceptor atom of OG-9. The more flexible side chain of this residue moves freely in the solution and generates polar contact in some instances with the ligand oxygen atom. Hydrogen bonding in the MD7 simulation shows that OG-3 is interacting with OD1 (carboxyl oxygen) and HN (amino hydrogen) atoms of Asp-23 and Gly-42 residues. Finally, the MD8 simulation with the same number of OG monomers as MD7 shows no hydrogen bonding pattern (with average lifetime cutoff >50 ps) but only strong, long-lived water bridges between hydroxyl atoms of the OG-4 and Asn-78, and Tyr-219 residues of the lectin. In spite of the ligand molecules used in the simulations were not constrained and were allowed to move freely in the solution; the interaction and hydrogen bonding patterns calculated from these simulations were qualitatively in good agreement with other theoretical works [4,26].

### 3.5. Diffusion coefficients of solvent and ligand molecules

From the structural analysis of the lectin it is evident that the properties of the water and ligand molecules at the binding site are distorted by the lectin residues and their flexible conformations dictate largely to the surrounding environment [52]. The motions concerned with the OG monomer are of prime importance for studying the dynamic properties of detergents used in the solubilization process. Translational diffusion coefficients ($D$) were calculated from Einstein's mean square displacement function for the water, OG monomers, and ions in the periodic box (Table 5). Since the concentrations of OG in the simulations are very close to the critical micelle concentration, it is fully acceptable to use the mean square displacement function to

Table 5
Diffusion coefficients calculated from the mean square displacement equation for the solvent molecules, OG monomers and different ions

| MD simulation | $D_{water}$ $10^{-9}$ $m^2/s$ | $D_{mon}$ [a] $10^{-9}$ $m^2/s$ | $D_{avg}$ [b] ($D_{hd}$) [c] $10^{-9}$ $m^2/s$ | $D_{Ca^{2+}}$ $10^{-9}$ $m^2/s$ | $D_{Mn^{2+}}$ $10^{-9}$ $m^2/s$ | $D_{Cl^-}$ $10^{-9}$ $m^2/s$ |
|---|---|---|---|---|---|---|
| MD1 | 5.4 | 1.6 | 0.7 (0.7) | 1.3 | 1.4 | 3.0 |
| MD2 | 5.4 | 1.2 | 1.2 (1.2) | 1.2 | 1.1 | 3.2 |
| MD3 | 5.4 | 0.9 | 0.9 (1.1) | 1.1 | 1.4 | 3.3 |
| MD4 | 5.4 | 2.5 | 1.0 (1.0) | 1.1 | – | 3.4 |
| MD5 | 5.5 | 1.1 | 1.1 (1.0) | – | 1.5 | 3.2 |
| MD6 | 4.9 | 0.9 | 0.9 (0.9) | – | – | – |
| MD7 | 5.4 | 1.1 | 0.7 (0.7) | 0.7 | 1.0 | 3.5 |
| MD8 | 5.4 | 1.1 | 0.8 (0.7) | 1.9 | 1.2 | 3.3 |
| MD9 | 5.6 | 0.7 | 0.7 (0.6) | 2.3 | 1.7 | 2.5 |
| MD10 | 5.4 | 1.3 | 0.9 (0.8) | 0.9 | 1.7 | 5.8 |

[a] Free OG monomer in the bulk solution which is far away from the lectin monomer.
[b] Average monomer diffusion coefficient of OG monomers in the solution.
[c] Average OG head group diffusion.

calculate the diffusion coefficients. As shown in Table 5, the diffusion coefficient of water molecules from different simulations are on average $5.4\times10^{-9}$ $m^2/s$, except MD6 simulation without any ions. It should be noted that in general the performance of the TIP3P water model by itself deviates from the experimental viscosity and diffusion coefficients by a factor of 2.8 and 2.2 [38,53]. The reported average values for the viscosity and diffusion coefficient from the TIP3P by the electrostatic Ewald summation method are 0.35 cP and $5.4\times10^{-9}$ $m^2/s$ [53]. The calculated $D$ for the water molecules in the present simulations do indeed overlap very well with previous work on the TIP3P water model. Interestingly, the diffusion coefficient of water in the MD6 simulation is much lower than in the other MD simulations. It is not proved, however we suspect that the presence of OG monomers without divalent ions in the protein simulations lowers the diffusion coefficients of water.

Based on distance from the center of the lectin, the OG monomer lying furthest away from the lectin surface was selected in each simulation and its free motion in the bulk solvent was calculated. This showed that individual monomer diffusion ($D_{mon}$) is independent of positions visited in the simulations performed in a large solvent periodic box (Table 5). Moreover their average diffusion with the other OG monomers presented in the fourth column of Table 5, gives some meaningful results ($D_{avg}$). The diffusion coefficients calculated for the OG head group (shown in parentheses in Table 5) also synchronizes with their average monomer diffusion. The average diffusion of the monomers in the MD1 simulation was much lower than their individual monomers because 50% of the monomers in the solution are in the micelle aggregate, thus hindering the motion of OG. The slow motion of these monomers included in the analysis with monomers having higher diffusion lowers the average diffusion of OG in the MD1 simulation. To further investigate the diffusion constants in this simulation the monomers in the aggregate and in the free solution were calculated individually to verify the influence of their $D$ values. As is evident from Table 6, the $D$ values are affected for the monomers in the micelle aggregate. The $D$ values were lower by approximately 2–3 times in the aggregate than in the free monomer state. Moreover, the OG monomer on the binding site was reduced to one-fifth of the value of the free monomer diffusion in the solution.

Table 6
Comparison of diffusion coefficients of OG monomers in the free solution, micelle aggregate, and at the lectin binding site in the MD1 simulation

| Free OG monomers | $D_{free}$ $10^{-9}$ $m^2/s$ | Aggregated OG monomers | $D_{aggregate}$ $10^{-9}$ $m^2/s$ |
|---|---|---|---|
| OG-1 | 1.6 | OG-3 | 0.8 |
| OG-2 | 1.4 | OG-6 | 0.5 |
| OG-4 | 0.8 | OG-8 | 0.7 |
| OG-5 | 1.1 | OG-9 | 1.0 |
| OG-7 | 1.6 | OG-10 | 0.9 |
| OG-11 | 1.1 | OG 12 | 0.5 |
| OG 14 | 1.5 | OG 13 | 0.6 |
| OG 17 | 1.2 | OG 15 | 0.8 |
| OG 19 | 1.0 | OG 18 | 0.6 |
| | | OG 20 | 0.5 |
| | | OG 16 | 0.3 |

The diffusion coefficients of the divalent $Ca^{2+}$ and $Mn^{2+}$ ions and the monovalent $Cl^-$ ion in the simulations are also very well reproduced, except in simulations MD9 and MD10 (Table 5). The $Ca^{2+}$ diffusion coefficient reported in the literature is $0.8–1.0\times10^{-9}$ $m^2/s$ [51]. This value is comparable to our MD simulations (Table 5) carried out in this work. Similarly $Mn^{2+}$ diffusion coefficients were also stable in the simulations and can be compared to the dynamics of calcium ions. The calculated $D$ values for the chloride ions are a little higher than the experimental value of $2.03\times10^{-9}$ $m^2/s$ [41]. A chloride $D$ value approximately twice higher was calculated in MD10 compared to the other MD simulations. The deviations in $D$ values for the ions in the MD9 and MD10 simulations can be attributed to the lack of proper ion–ion dipole interactions; in addition, calcium ions have a low affinity for water, which might cause them to move around more randomly in the bulk solution than the manganese ions [51]. As stated above the water model by itself overshoots the experimental $D$ values; although the $D$ values calculated for the OG monomers in this work are at very low concentrations (Table 1). They might need a correction factor to compare the results with the higher concentrated experiments [30].

Improvement in the performance of the dynamic properties of the OG can be achieved from the new TIP4P-Ew water model with the application of the Particle–Mesh–Ewald summation method [38,54]. The addition of a new fictitious site (acting as an interaction center in the water model) at the center of the bisector of the H–O–H angle improves the dynamic properties of the biomolecular systems when compared to the previous three-site water models. We are currently testing these water potentials with the CHARMM parameters [32] for the investigation of glycolipid properties. The only limitation to this model is the computation time. Longer computing times are expected in the four-site model than the water model used in this work because of the extra atom in the model [54]. The preliminary results calculated with TIP4P-Ew for the diffusion coefficient of water are in excellent agreement with the experimental values. The $D$ values of 2.4 and $2.5\times10^{-9}$ $m^2/s$ (results not yet published) have been calculated with these potentials for the solvent molecules. The experimental value for the self-diffusion coefficient of water reported in the literature is $2.4\times10^{-9}$ $m^2/s$ [26]. In addition, the model has been tuned to work efficiently with the protein force field parameters to reproduce the interfacial thermodynamic and kinetic properties.

## 4. Conclusions

In the present work molecular dynamics simulations are applied to study the properties of pea (*P. sativum*) lectin with OG ligands. Ten different simulations performed on pea lectin/OG systems reveal the structure, dynamics, and interaction properties of these molecules in an explicit solvent environment. This work facilitates the understanding of lectin interactions with glycolipid molecules and is also very useful for the study of complex interactions involved in the solubilization

process of proteins with detergents. Because there were no prior concrete results reported on the specific interaction or binding analysis of pea lectin we tried to address these issues from the MD simulations in a realistic manner employing a fully solvated lectin monomer applied with periodic boundary conditions, different combinations of OG monomers, and $Ca^{2+}$, $Mn^{2+}$, and $Cl^{-}$ ions. Moreover, none of the molecular components in the periodic cell were constrained; different initial coordinates and random velocities, and higher nonbonded cutoffs for the van der Waals interactions and Particle–Mesh–Ewald summation method for treating the electrostatic interactions were used in the simulations. The approach followed in solving such systems seems to provide more information and clues about biomolecular structure and function than the single long simulation performed with either unconstrained or partly constrained molecular entities [27].

The stability in the overall conformation of a lectin was conserved in all the simulations. Slightly higher deviations were observed in the simulation with two OG monomers and divalent ions, but the deviations in this system were decreased after a few hundred picoseconds once the lectin structure in the solution was fully relaxed. Despite independent MD runs started from different initial conditions the global conformations of the lectin fairly converged to the stable state in all the simulations. The size of the pea lectin determined from the radius of gyration reached constant at the early stage and remained steady throughout the simulations. The RMS fluctuations per residue in the lectin backbone and side chains with reference to the average solution structure from the trajectories were constant with the simulations. The dynamics in the lectin residues were calculated from the B-factor distribution and compared to the crystal structure derived from the X-ray diffraction studies [42]. Most of the peaks observed in the crystal structure were also retained in the simulations, indicating the high quality of the models applied in the simulations [13]. Few regions in the MD simulations show higher peaks than the crystal structure B-factor results. The larger dynamics are occurred in the cyclic residues and the shallow region of the lectin at the interface to the solvent environment that are not well characterized in the diffraction crystal structure analysis.

Interaction energy analyses reported for the individual OG monomer and the pea lectin from the dynamic trajectories in each simulation indicate different binding sites of the lectin–ligand complex. Each OG monomer interacting with the amino acid residues was calculated and it was found that binding was facilitated by the favourable specific electrostatic interactions between the lectin and the OG monomer. The contributions from these specific (e.g., electrostatic and hydrogen bond) and also nonspecific (van der Waals) interactions are the primary driving force for the stable ligand–lectin complex formed in solution. This proves that a lock-and-key description of the pea lectin with the OG monomer was not appropriate. The local conformation of the lectin might flexibly adapt to the surrounding environment [25] and accommodate the visiting ligand molecule. The binding process in such systems work closer to the induced-fit principle [18]. Interestingly, the simulation with 20 OG monomers shows the binding site very close to the crystal structure site reported by Pletnev et al. [13]. The OG-16 monomer head group interacts strongly with the lectin residues Tyr-100, Leu-101, Ala-107, Glu-108, and Lys-145. The $Ca^{2+}$ divalent ion was also found near the carbohydrate binding site. The elaborate study of the interactions of lectin system with detergent molecules in aqueous solution can also be visualized in terms of free energy calculations [4,19,23].

In addition, multiple strong interactions of OG with the lectin were seen in the simulation with only $Ca^{2+}$ ions. This indicates that $Ca^{2+}$ ions, without $Mn^{2+}$ ions in the solution, simply bind to the lectin [51]. As is evident from the simulations with both divalent ions, it seems the inclusion of $Mn^{2+}$ divalent ions compensates for the effect of multiple bindings of OG to the lectin. Intriguingly, the MD simulation without any ions in the solution verified no binding of OG to the lectin monomer. This demonstrates the importance of divalent ions for the ligand–lectin binding processes. As they are the essential parts of most leguminous lectins the investigations proved the necessity of $Ca^{2+}$ for the biological activity of the lectins. These results also suggest the performance of CHARMM parameters employed in the simulations to analyze such effects [32].

The inherent nature of detergents self-assembling into molecular aggregates of a small micelle was apparent in the simulation with 20 OG monomers (Fig. 7). About 9–10 monomers in the solution joined together at the lectin surface and started to build a micelle. The hydrocarbon chains were facing inside the micelle along with the lectin hydrophobic side chain residues, thus these OG tails were prevented from interacting with the rest of the aqueous polar environment [50]. The OG-8 monomer head group was pushed into the proton cloud of Thr-192 and Asp-195 lectin residues with an increase in the electrostatic interaction energy. The tail of this monomer was held tightly with the high hydrophobic residues of Val-172, Leu-173, and Val-196 in the lectin–micelle hydrophobic center. The center of geometry of the OG monomer tails involved in the micelle were analyzed on the basis of their distances with respect to the OG-8 monomer (foundation for the micelle building process) before and after the formation of the micelle (Table 3) from the trajectories. The results found that the distance to this center was decreased after the micelle was formed on the lectin surface. In addition, the influence of the diffusion coefficients for these monomers was affected by a 2–3-fold decrease in their $D$ values (Table 6) after micellization.

The solvent accessible surface area of the lectin structures indicates that the surface is loose and has plenty of cavities where it can effectively interact with the solvent molecules. The calculated average surface area from all simulations is $11.2 \times 10^3$ Å$^2$, which is higher than the crystal structure value of $9.2 \times 10^3$ Å$^2$. The major contribution to this comes from the β-side chains, where most of these residues are in direct contact with the water (Table 2). The water staying next to the lectin thus participates in hydrogen bonding and water bridges to the surface residues and stabilizes the overall structure of the lectin [26,50]. Improved hydrogen bonding patterns and water bridges between the lectin and OG were identified from the simulations performed in a large solvent periodic box. Finally, the diffusion coefficients calculated for the water molecules are in good agreement with the

standard $D$ values reported for the TIP3P water model. An average $D$ value of $5.4\times10^{-9}$ $m^2/s$ was calculated for the solvent molecules in the present simulations and this is comparable to the $D$ value of $5.2\times10^{-9}$ $m^2/s$ reported in the literature [38,53]. In addition, diffusion coefficients for the individual OG monomers in solution were calculated and averaged over the total number of OG monomers present in the respective simulations. Comparing the average $D$ values of the OG monomers provided a good correlation between their $D$ values in different simulations. The diffusion coefficients calculated for the ions were also consistent with the experimental results reported in the literature [41,51]. The ligand–lectin properties reported in this work lead to the conclusion that the applied molecular models were more realistic and the force field parameters were appropriate to explain the phenomenological behaviour observed in the experiments for these macromolecules.

## References


[1] N. Sharon, H. Lis, Lectins: cell-agglutinating and sugar-specific proteins, Science 177 (1972) 949–959.

[2] S. Kawai, I. Takeuchi, Concanavalin A-induced agglutination and binding of Con A to the differentiating cells of *Dictyostelium discoideum*, Dev. Growth Differ. 18 (1976) 311–317.

[3] A. Poveda, J. Jimenez-Barbero, NMR studies of carbohydrate–protein interactions in solution, Chem. Soc. Rev. 27 (1998) 133–143.

[4] R.A. Bryce, I.H. Hillier, J.H. Naismith, Carbohydrate–protein recognition: molecular dynamics simulations and free energy analysis of oligosaccharide binding to Concanavalin A, Biophys. J. 81 (2001) 1373–1388.

[5] J.R. Grigera, Molecular dynamics simulation of ligand-receptor studies. Carbohydrates interaction in aqueous solutions, Curr. Pharm. Des. 8 (2002) 1579–1604.

[6] D. Gupta, T.K. Dam, S. Oscarson, C.F Brewer, Thermodynamics of lectin–carbohydrate interactions, J. Biol. Chem. 272 (1997) 6388–6392.

[7] H.-J. Gabius, Probing the cons and pros of lectin-induced immunomodulation: case studies for the mistletoe lectin and galectin-1, Biochimie 83 (2001) 659–666.

[8] T.W. Hamelryck, R. Loris, J. Bouckaert, L. Wyns, Properties and structure of the legume lectin family, Trends Glycosci. Glycobiol. 10 (1998) 349–404.

[9] I.S. Trowbridge, Isolation and chemical characterization of a mitogenic lectin from *Pisum sativum*, J. Biol. Chem. 249 (1974) 6004–6012.

[10] E.J. Meehan, J. McDuffie, H. Einspahr, C.E. Bugg, F.L. Suddath, The crystal structure of pea lectin at 6- resolution, J. Biol. Chem. 257 (1982) 13278–13282.

[11] H. Einspahr, E.H. Parks, K. Suguna, E. Subramanian, F.L. Suddath, The crystal structure of pea lectin at 3.0- resolution, J. Biol. Chem. 261 (1986) 16518–16527.

[12] F.P. Schwarz, K.D. Puri, R.G. Bhat, A. Surolia, Thermodynamics of monosaccharide binding to Concanavalin A, pea (*Pisum sativum*) lectin, and lentil (*Lens culinaris*) lectin, J. Biol. Chem. 268 (1993) 7668–7677.

[13] V.Z. Pletnev, S.N. Ruzheinikov, I.N. Tsygannik, I.Y. Mikhailova, W. Duax, D. Gosh, W. Pangborn, The structure of pea lectin-D-glucopyranose complex at a 1.9 resolution, Russ. J. Bioorgan. Chem. 23 (1997) 436–445.

[14] P. Konidala, L.-Z. He, B. Niemeyer, Molecular dynamics characterization of *n*-octyl-β-D-glucopyranoside micelle structure in aqueous solution, J. Mol. Graph. Model. 25 (2006) 77–86.

[15] L.-Z. He, V. Garamus, B. Niemeyer, H. Helmholz, R. Willumeit, Determination of micelle structure of octyl-β-glucoside in aqueous solution by small angle neutron scattering and geometric analysis, J. Mol. Liq. 89 (2000) 239–249.

[16] M. le Maire, P. Champeil, J.V. Moller, Interaction of membrane proteins and lipids with solubilizing detergents, Biochim. Biophys. Acta 1508 (2000) 86–111.

[17] F.P. Schwarz, S. Misquith, A. Surolia, Effect of substituent on the thermodynamics of D-glucopyranoside binding to Concanavalin A, pea (*Pisum sativum*) and lentil (*Lens culinaris*) lectin, Biochem. J. 316 (1996) 123–129.

[18] B. Ma, S. Kumar, C.-J. Tsai, H. Wolfson, N. Sinha, R. Nussinov, Encyclopedia of life sciences, in: S. Robertson (Ed.), Protein–Ligand Interactions: Induced Fit, Macmillan Publishers Ltd, London, UK, 2001, p. 1.

[19] S. Sen, L. Nilsson, Free energy calculations and molecular dynamics simulations of wild-type and variants of the DNA–*Eco*RI complex, Biophys. J. 77 (1999) 1801–1810.

[20] S. Yan, M. Wu, D.J. Patel, N.E. Geacintov, S. Broyde, Simulating structural and thermodynamic properties of carcinogen-damaged DNA, Biophys. J. 84 (2003) 2137–2148.

[21] D. Neumann, O. Kohlbacher, H.-P. Lenhof, C.-M. Lehr, Lectin–sugar interaction: calculated versus experimental binding energies, Eur. J. Biochem. 269 (2002) 1518–1524.

[22] C.M. Reyes, R. Nifosi, A.D. Frankel, P.A. Kollman, Molecular dynamics and binding specificity analysis of the bovine immunodeficiency virus BIV Tat–TAR complex, Biophys. J. 80 (2001) 2833–2842.

[23] T. Lazaridis, Binding affinity and specificity from computational studies, Curr. Org. Chem. 6 (2002) 1319–1332.

[24] S. Kumar, R. Nussinov, Close-range electrostatic interactions in proteins, Chem. Biol. Chem. 3 (2002) 604–617.

[25] H. Jang, P.S. Crozier, M.J. Stevens, T.B. Woolf, How environment supports a state: molecular dynamics simulations of two states in bacteriorhodopsin suggest lipid and water compensation, Biophys. J. 87 (2004) 129–145.

[26] S. Sen, L. Nilsson, Structure, interaction, dynamics and solvent effects on the DNA–*Eco*RI complex in aqueous solution from molecular dynamic simulation, Biophys. J. 77 (1999) 1782–1800.

[27] M. Karplus, J.A. McCammon, Molecular dynamics simulations of biomolecules, Nat. Struct. Biol. 9 (2002) 646–652.

[28] L. Saiz, M.L. Klein, Computer simulation studies of model biological membranes, Acc. Chem. Res. 35 (2002) 482–489.

[29] B.R. Brooks, R.E. Bruccoleri, B.D. Olafson, D.J. States, S. Swaminathan, M. Karplus, CHARMM: A program for macromolecular energy, minimization, and dynamics calculations, J. Comput. Chem. 4 (1983) 187–217.

[30] A.M. Dixon, R.M. Venable, R.W. Pastor, T.E. Bull, Micelle-bound conformation of a hairpin-forming peptide: combined NMR and molecular dynamics study, Biopolymers 65 (2002) 284–298.

[31] W.L. Jorgensen, J. Chandrasekhar, J.D. Madura, R.W. Impey, M.L. Klein, Comparison of simple potential functions for simulating liquid water, J. Chem. Phys. 79 (1983) 926–935.

[32] A.D. MacKerell Jr., D. Bashford, M. Bellott, R.L. Dunbrack Jr., J.D. Evanseck, M.J. Field, S. Fischer, J. Gao, H. Guo, S. Ha, D. Joseph-McCarthy, L. Kuchnir, K. Kuczera, F.T.K. Lau, C. Mattos, S. Michnick, T. Ngo, D.T. Nguyen, B. Prodhom, W.E. Reiher III, B. Roux, M. Schlenkrich, J.C. Smith, R. Stote, J. Straub, M. Watanabe, J. Wiorkiewicz-Kuczera, D. Yin, M. Karplus, All-atom empirical potential for molecular modeling and dynamics studies of proteins, J. Phys. Chem., B 102 (1998) 3586–3616.

[33] M. Kuttel, J.W. Brady, K.J. Naidoo, Carbohydrate solution simulations: producing a force field with experimentally consistent primary alcohol rotational frequencies and populations, J. Comput. Chem. 23 (2002) 1236–1243.

[34] R. Palma, M.E. Himmel, G. Liang, J.W. Brady, in: M.E. Himmel (Ed.), Glycosyl Hydrolases in Biomass Conversion, Molecular Mechanics Studies of Cellulases, vol. 769, American Chemical Society, Washington DC, 2001, p. 112.

[35] S.N. Ha, A. Giammona, M. Field, J.W. Brady, A revised potential-energy surface for molecular mechanics studies of carbohydrates, Carbohydr. Res. 180 (1988) 207–221.

[36] Z. Li, T. Lazaridis, The effect of water displacement on binding thermodynamics: Concanavalin A, J. Phys. Chem., B 109 (2005) 662–670.

[37] J.P. Ryckaert, G. Ciccotti, H.J.C. Berendsen, Numerical integration of the cartesian equation of motion of a system with constraints: molecular dynamics of *n*-alkanes, J. Comput. Phys. 23 (1977) 327–341.

[38] U. Essmann, L. Perera, M.L. Berkowitz, T. Darden, H. Lee, L.G.J. Pedersen, A smooth particle mesh Ewald method, J. Chem. Phys. 103 (1995) 8577–8593.

[39] W.G. Hoover, Canonical dynamics: equilibrium phase-space distributions, Phys. Rev., A 31 (1985) 1695–1697.
[40] D. Beglov, B. Roux, Finite representation of an infinite bulk system: solvent boundary potential for computer simulations, J. Chem. Phys. 100 (1994) 9050–9063.
[41] W. Wriggers, E. Mehler, F. Pitici, H. Weinstein, K. Schulten, Structure and dynamics of calmodulin in solution, Biophys. J. 74 (1998) 1622–1639.
[42] Z. Yuan, T.L. Bailey, R.D. Teasdale, Prediction of protein B-factor profiles, Proteins: Struct. Funct. Bioinf. 58 (2005) 905–912.
[43] M.F. Gerini, D. Roccatano, E. Baciocchi, A. Di Nola, Molecular dynamics simulations of lignin peroxidase in solution, Biophys. J. 84 (2003) 3883–3893.
[44] B. Lee, F.M. Richards, The interpretation of protein structures: estimation of static accessibility, J. Mol. Biol. 55 (1971) 379–400.
[45] T. Wymore, T.C. Wong, Molecular dynamics study of substance P peptides partitioned in a sodium dodecylsulfate micelle, Biophys. J. 76 (1999) 1213–1227.
[46] R.M. Garavito, D. Picot, P.J. Loll, Strategies for crystallizing membrane proteins, J. Bioenerg. Biomembranes 28 (1996) 13–26.
[47] C. Ostermeier, H. Michel, Crystallization of membrane proteins, Curr. Opin. Struct. Biol. 7 (1997) 697–701.
[48] J.-L. Eisele, J.P. Rosenbusch, Crystallization of porin using short chain phospholipids, J. Mol. Biol. 206 (1989) 209–212.
[49] J. Lauterwein, C. Bösch, L.R. Brown, K. Wüthrich, Physicochemical studies of the protein–lipid interactions in melittin-containing micelles, Biochim. Biophys. Acta 556 (1979) 244–264.
[50] S. Bogusz, R.M. Venable, R.W. Pastor, Molecular dynamics simulations of octyl glucoside micelles: structural properties, J. Phys. Chem., B 14 (2000) 5462–5470.
[51] D.E. Clapham, Calcium signaling, Cell 80 (1995) 259–268.
[52] C.D. Bruce, S. Senapati, M.L. Berkowitz, L. Perera, M.D.E. Forbes, Molecular dynamics simulations of sodium dodecyl sulfate micelle in water: the behaviour of water, J. Phys. Chem., B 106 (2002) 10902–10907.
[53] S.E. Feller, R.W. Pastor, A. Rojnuckarin, S. Bogusz, B.R. Brooks, Effect of electrostatic force truncation on interfacial and transport properties of water, J. Phys. Chem. 100 (1996) 17011–17020.
[54] H.W. Horn, W.C. Swope, J.W. Pitera, J.D. Madura, T.J. Dick, G.L. Hura, T. Head-Gordon, Development of an improved four-site water model for biomolecular simulations: TIP4P-Ew, J. Chem. Phys. 120 (2004) 9665–9678.